


Adapting the PyCBC pipeline to find and infer the properties of gravitational waves from massive black hole binaries in LISA

Connor R. Weaving¹ , Laura K. Nuttall¹ , Ian W. Harry¹ ,
Shichao Wu²  and Alexander Nitz^{3,2} 

¹ University of Portsmouth, Portsmouth, PO1 3FX, United Kingdom

² Max-Planck-Institut für Gravitationsphysik (Albert-Einstein-Institut), D-30167
Hannover, Germany

³ Department of Physics, Syracuse University, Syracuse NY 13244, USA

Abstract. The Laser Interferometer Space Antenna (LISA), due for launch in the mid 2030s, is expected to observe gravitational waves (GW)s from merging massive black hole binaries (MBHB)s. These signals can last from days to months, depending on the masses of the black holes, and are expected to be observed with high signal to noise ratios (SNR)s out to high redshifts. We have adapted the PyCBC software package to enable a template bank search and inference of GWs from MBHBs. The pipeline is tested on the LISA data challenge (LDC)’s Challenge 2a (“Sangria”), which contains MBHBs and thousands of galactic binaries (GBs) in simulated instrumental LISA noise. Our search identifies all 6 MBHB signals with more than 98% of the optimal signal to noise ratio. The subsequent parameter inference step recovers the masses and spins within their 90% confidence interval. Sky position parameters have 8 high likelihood modes which are recovered but often our posteriors favour the incorrect sky mode. We observe that the addition of GBs biases the parameter recovery of masses and spins away from the injected values, reinforcing the need for a global fit pipeline which will simultaneously fit the parameters of the GB signals before estimating the parameters of MBHBs.

1. Introduction

In preparation for the Laser Interferometer Space Antenna (LISA) [1] launch in the mid 2030's, considerable efforts are being made to design and develop the data analysis tools needed to extract and examine the numerous different types of gravitational wave (GW) signals expected to be found in the LISA band. LISA will probe the mHz GW spectrum, allowing us to explore sources such as massive black hole binaries (MBHB) with total mass between $10^5 - 10^8 M_\odot$ [2]; intermediate-mass black hole binaries (IMBHB) with total masses in the range $10^2 - 10^5 M_\odot$ [3]; extreme mass-ratio and intermediate mass-ratio inspirals (EMRI and IMRI) where coalescences have mass ratios of $10^{-6} - 10^{-3}$ and $10^{-3} - 10^{-1}$ respectively, with total masses in the range $10^3 - 10^7 M_\odot$ [4, 5], and more. Each of these systems, if detected and analysed properly, will help constrain and test a wide range of theories, such as the effect of dark matter on a GW propagating from a MBHB, or testing General Relativity by constraining the deviation from the Kerr metric using EMRIs (for example see Ref [6]). Depending on the model from which the MBHBs population has been generated and whether or not they are joint observations with other detectors such as pulsar timing arrays, the merger rate is estimated to be from $O(2) - O(100) \text{ yr}^{-1}$ [7–10].

In order to ensure that we can detect and analyse these signals, the LISA data challenge (LDC) [11, 12], generates mock LISA data with various GW signals injected into simulated LISA noise. The series of challenges will eventually replicate all of the complexities that the true LISA data will contain, such as gaps in the data; noise artefacts found within the data that will affect the ability to infer a system's parameters; LISA's true orbital position as the detector response due to the longer, lower frequency GW signals are time dependent on LISA's position; a time varying estimate of the noise to account for longer, GW signals. All of these issues will need to be addressed before LISA data can be analysed. Several groups are working on different aspects of LISA data analysis and their work is highlighted in Refs [13–22].

In this paper, we present our pipeline which was developed to analyse the second LDC, referred to as “Sangria” [23, 24]. This data set is a blind data challenge, where there are an unknown number of injected GW signals hidden in Gaussian instrumental noise. There are two types of GW signals injected into Sangria. The first type of signal is galactic white dwarf binaries (GBs) [25] which are expected to be the most abundant source of GW signals to be present in LISA data. The accumulation of these signals forms a “confusion noise” which dominates the $0.5 - 3 \text{ mHz}$ range of the frequency spectrum. A subset of these are known as verification binaries (VBs) [26], which are signals that are known in advance due to electromagnetic observations. The second type of signal in the data are MBHBs. These are generated using the IMRPhenomD waveform model [27, 28]. IMRPhenomD produces two GW polarizations which encode the effect a GW has on the relative distance between particles, the derivation of which is well known and can be found in Ref [29]. These polarizations are then projected onto the LISA constellation to produce an arm response. The arm response from LISA is known

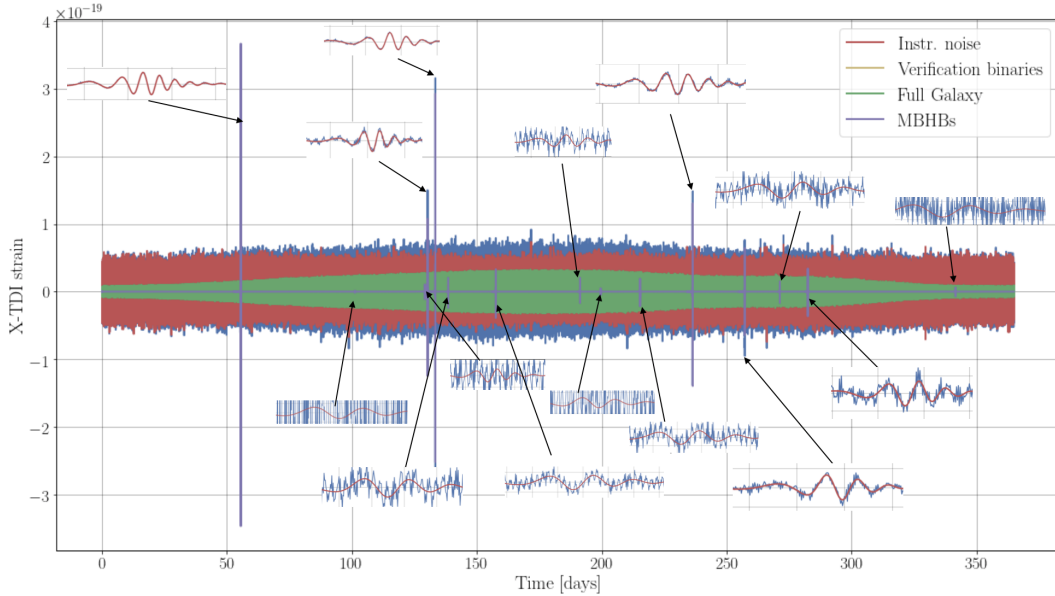


Figure 1. Timeseries of X TDI variable from the Sangria training data set. The data consists of a year’s worth of data sampled at 5s, with 15 MBHB signals injected into the data. This data also contains Gaussian instrumental noise, 30 million GBs, of which 17 are VBs. This image was taken from the LDC website for the Sangria challenge in Ref [23].

to be dominated by laser frequency noise and therefore Time Delayed Interferometry (TDI) [30, 31] techniques must be used in order to extract GW information from the raw data streams. The Michelson TDI variables X, Y and Z are provided in this data challenge.

The data set spans a year’s worth of data sampled at 5 seconds, which is the expected sample rate for LISA. Figure 1 shows a time series of the X TDI data stream of the Sangria training data set. An overview of previous LDCs can be found in Refs [32–34].

The tools used in our analysis have been developed within PyCBC [35]. PyCBC is an open source GW data analysis software package and is one of the main pipelines used to detect and characterise compact binary mergers from LIGO, Virgo and KAGRA (LVK) detectors [36–40]. PyCBC has been used to detect and analyse $\mathcal{O}(100)$ GW signals from compact binary mergers to date, an overview of which can be found in Refs [41–43]. We have adapted the techniques developed for LVK searches and applied them to LISA-like signals, in this case MBHBs.

It is important to note that there is far more work to do to achieve a reliable analysis of MBHBs in realistic conditions. The tools made available through this paper are a first attempt at the bigger picture solution, which will require many more iterations before being considered “production ready”.

The tools made available through this paper are a first attempt to search for and infer the properties of MBHBs using the PyCBC framework. There is further work

needed to make these tools production ready in realistic conditions. The paper is laid out as follows. In Section 2, we introduce PyCBC and the components which make up our pipeline. We give the basic details needed to understand how PyCBC approaches each stage of detecting and recovering GW system parameters. In Section 3, we outline how we have adapted PyCBC in order to detect and infer MBHBs. In Section 4, we present the results of each stage of our development leading to the analysis of the blind Sangria data. Finally in Section 5 we discuss the challenges in developing these tools, future work and our conclusions.

2. PyCBC: Search and inference

We can split the PyCBC analysis pipeline up into two distinct sections, the search and the inference. The search portion of the pipeline is responsible for identifying candidate GW signals within the data, and the inference portion returns a statistical estimate of the parameters of the GW signals identified. Below we outline which tools within PyCBC have been used and adapted for MBHB signals.

2.1. The search

The main component of the search is the application of matched filtering. The matched filter signal-to-noise ratio (SNR) is designed to indicate when a particular signal we are searching for could be present in data [44]. For data in the form $d(t) = s(t) + n(t)$, where $s(t)$ is a signal and $n(t)$ is the detector noise, we choose a linear filter, $F(t)$, such that the output of the correlation of a signal's template with the data itself is the matched filter. Matched filtering allows the maximisation of the SNR, ρ , defined in Equation 1 below.

$$\phi(t) = \int_{-\infty}^{\infty} F(t - \tau) d(\tau) d\tau = \int_{-\infty}^{\infty} F^*(\tau) d(\tau) d\tau = \phi_h + \phi_n, \quad \rho = \frac{|\phi_h^2|}{E\{|\phi_n^2|\}} \quad (1)$$

where ϕ_h and ϕ_n are the signal and noise components of the matched filter respectively and E is the expectation value.

We use a model for our templates, $h(t)$, which represents the response of a detector given a GW passing through the instrument. PyCBC can project the GW polarizations produced by varying waveform models onto different ground-based detectors to return an arm response. For some GW emitting systems, many parameters are required to define the full signal response. Given such a broad parameter space of values to explore, we require a large amount of templates to search the data in order to potentially detect a GW. It is not optimal to create a bank over a high number of parameters, so a reduced parameter space is used to generate a bank [45]. PyCBC generates template banks which can contain $\mathcal{O}(100,000)$ templates for a LVK-like search to effectively explore the GW parameter space in question. Details of the various methods used to generate

template banks can be found in Refs [46–50]. When generating a template bank, the match, as defined in Equation 2, is computed between templates.

$$\mathcal{M}(s_1, s_2) = \max_{\phi_c, t_c} \left[4\Re \int_0^\infty \frac{\tilde{s}_1^*(f) \tilde{s}_2(f)}{S_n(f)} df \right], \quad (2)$$

given two templates s_1 and s_2 , the match tells us how similar to each other these templates are whilst maximising over the coalescence time t_c and the phase at coalescence ϕ_c . $S_n(f)$ is the one-sided power spectral density (PSD). Templates are first normalized such that the inner product, defined in Equation 3, gives $(s_1|s_1) = 1$. Using the normalized templates in the match returns a number in the range $[0,1]$ where 1 states that the two normalized templates are identical.

$$(s_1|s_2) = 4\Re \int_0^\infty \frac{\tilde{s}_1^*(f) \tilde{s}_2(f)}{S_n(f)} df. \quad (3)$$

Maximizing Equation 2 over t_c implies that we do not take into consideration the varying response function from LISA over time, given the fact the antennas sky position is changing within the duration of the MBHB signal. However, because the majority of the SNR from merging MBHBs is within the final $\mathcal{O}(\text{day})$, and these systems have SNRs $\mathcal{O}(1000)$, we are safe to assume LISA is approximately stationary during this time period.

Under the assumption the noise is both stationary and Gaussian we define S_n through

$$\langle \tilde{n}(f) \tilde{n}^*(f') \rangle = \frac{1}{2} S_n(|f|) \delta(f - f'), \quad (4)$$

where $f \geq 0$ and the square brackets represent the ensemble average.

The matched filter is then applied to all templates and the data we are searching over, giving an SNR timeseries per template. Each timeseries is then passed to a clustering algorithm, to return the highest SNR template per time in the data. A trigger is defined by a peak in the SNR timeseries reaching, or surpassing, a certain threshold. Additional stages are then applied to search for coincidences over multiple detectors and calculate their significance [37, 51].

2.2. The inference

PyCBC can infer signal parameters through sampling the posterior probability defined by Bayes theorem

$$p(\theta|d) = \frac{\mathcal{L}(d|\theta)p(\theta)}{p(d)} \quad (5)$$

where $\mathcal{L}(d|\theta)$ is the likelihood of the data d given the parameters θ , $p(\theta)$ is the prior of the parameters and $p(d)$ is the evidence and θ represents an integer N number of

parameters $\underline{\theta} = \{\theta_1, \dots, \theta_N\}$. The main component of Equation 5 to compute is the likelihood which under the assumptions of Gaussianity and stationarity takes the form:

$$\log \mathcal{L}(d, \underline{\theta}) \propto (d|s_\theta) - \frac{1}{2}(s_\theta|s_\theta) - \frac{1}{2}(d|d), \quad (6)$$

where $s_\theta \equiv s(\underline{\theta})$.

We can speed up likelihood calculations by enforcing some assumptions about our GW.

$$\tilde{h}(f; \underline{\theta}, \phi) = A(f, \underline{\theta}) \exp[i(\Psi(f, \underline{\theta}) + \phi)]. \quad (7)$$

We use IMRPhenomD (2,2) mode only signals, and express our GW strain, $\tilde{h}(f)$, as a function of a smoothly varying amplitude and phase, where f is frequency, $A(f, \underline{\theta})$ is the amplitude of the GW, Ψ is the phase of the waveform and ϕ is some arbitrary phase constant.

With the GW strain expressed in this form, we use the application of heterodyning (sometimes referred to as relative binning) which assumes a smooth signal which varies in amplitude and phase. Heterodyning is a signal processing technique used to separate data into low and high frequency components. Our inference application of heterodyning allows us to greatly speed up likelihood calculations by first finding a high likelihood template with our template bank search. The corresponding template is then used as a reference to explore the region of high likelihood. A derivation of this method applied to GWs can be found in Refs [52, 53].

In order to explore the parameter space, there are several samplers in PyCBC which implement different methods, including Markov Chain Monte Carlo (MCMC) and Nested Sampling. An overview of PyCBC's inference setup can be found in Ref [54].

3. Adapting PyCBC's search and inference for MBHBs

3.1. Templates

In order to perform a matched filter search, we need to be able to generate templates that represent LISA's arm response given a GW signal passing through the instrument. The data we are searching over is given in terms of TDI variables; we therefore must put the templates in this format.

A vital part of this development is the use and implementation of the open source software BBHx waveform generator [55–62], which we use to generate the expected strain from MBHB systems. BBHx generates the GW polarizations, projects them onto LISA to form an arm response and then creates the TDI. BBHx implements the IMRPhenomHM [36, 63] waveform model to produce GW polarizations which is based on IMRPhenomD, but includes other sub-dominant modes. In this work, we set the IMRPhenomHM to generate just the (2,2) mode in order to match the Sangria convention. We transform both the data and the TDI templates into noise independent data streams referred to as A, E and T [64] via the transforms in Equation 8.

$$A = (Z - X)/\sqrt{2}, \quad E = (X - 2Y + Z)/\sqrt{6}, \quad T = (X + Y + Z)/\sqrt{3}. \quad (8)$$

Parameter	Lower Bound	Upper Bound
M_T (M_\odot)	2×10^5	2×10^7
q	1	4
a_1, a_2	-0.99	0.99
t_c (s)	2628000	28908000
β (rad)	$-\pi/2$	$\pi/2$
λ (rad)	0	2π
ψ, ι (rad)	0	π

Table 1. The parameter ranges used to generate the template bank. This covers the full range of potential systems that are defined within the conventions of the Sangria challenge. M_T is detector frame total mass of the black holes; q is mass ratio where $m_1 > m_2$ and m_1 is the primary mass and m_2 the secondary; a_1 and a_2 are the aligned spins of the two black holes; t_c is time of coalescence; β is ecliptic latitude; λ is ecliptic longitude; ψ is polarization angle; ι is inclination.

The data streams A and E have equal SNR across the entire LISA frequency band. This is not true for the T TDI stream as at lower frequencies the SNR contribution from T does not compete with A and E. However, T does contribute SNRs that can be greater than A or E at higher frequencies in the LISA band and is therefore included in the inference analysis [64]. BBHx generates templates A, E and T in the same convention as in Equation 8.

3.2. Template bank

We generated a template bank of the A TDI data stream for our search. Due to the SNRs of MBHBs being so large, we populated a less dense template bank when compared with LIGO template bank searches to balance accuracy of the signal trigger time versus computation cost of producing the bank.

For the bank generation we use stochastic placement [65–67]. Specifically we use the PyCBC algorithm “brute bank” with the parameters defined in Table 1 and a minimal match of 0.7. The minimal match defines how densely the parameter space is sampled. For example, with a minimal match of 0.7, if any newly generated template matches with any other template in the bank above the minimal match, it is rejected and another template is generated. The process repeats until a pre defined number of templates have been rejected from the bank placement.

The luminosity distance D_L is marginalized over in the matched filter calculations. The time of coalescence is sampled with one month from the beginning and end of the year removed. This is to ensure no edge corruption artefacts are present in the data when performing matched filtering, which could cause false triggers. This resulted in a bank size of approximately 13,000 templates.

Parameter	Lower Bound	Upper Bound
M_c (M_\odot)	87055	8705505
q	1	4
a_1, a_2	-0.99	0.99
t_c (s)	$t_{ref} - 2$ days	$t_{ref} + 2$ days
$\cos \beta, \lambda, \psi$ (rad)	0	$\pi/2$
$\sin \iota$ (rad)	0	π
D_L (Mpc)	10^3	10^6

Table 2. A list of all parameters and their ranges given to the prior, $p(\theta)$. All of the parameter ranges are distributed uniformly.

3.3. Sampling, priors and sky folding

We sample the heterodyne likelihood using the Nested Sampling tool Dynesty [68]. Table 2 outlines the parameters used in the inference. Uniform priors are given to all parameters defined in Table 2. M_c is the chirp mass of the system [69].

When sampling within the LISA frame, there are 8 known degeneracies for sky location, four longitudinal at $\{\lambda + \frac{\pi}{2}(0, 1, 2, 3), \psi + \frac{\pi}{2}(0, 1, 2, 3)\}$ and two latitudinal at $\{\pm\beta, \pm\cos\iota, \pm\cos\psi\}$. Instead of sampling the entire parameter space, we restrict our sky location parameters to one of eight octants of the sky. After drawing a sample from our defined octant, we compute the likelihood at the other 7 modes. We then marginalise over the 8 likelihood values. A post-processing step is then implemented to “unfold” the sky positions by drawing randomly from each sample’s marginalized likelihood, giving us the sky position associated with that randomly drawn marginalized likelihood. This effectively samples the entire parameter space without having to sample other parts of the sky as we compute the likelihood directly at the analytical location of the other sky modes. The details of the degeneracies and sky modes are summarised in detail in Ref [59].

All samples for inference are taken within the LISA reference frame, not the solar system barycentre (SSB) frame, even though the injected parameters in Sangria are all with reference to the SSB frame. The reason for this is to break well known sky degeneracies, which are points of similar likelihood values in the sky, but also take advantage of known sky modes that are present when sampling in the LISA frame.

3.4. PSDs

When GBs are included in the data, we assume them to be part of the noise $n(t)$. As there are several thousands of these signals of varying amplitude and phase, we can justify their accumulation to be Gaussian (but not stationary) by the central limit theorem. When constructing the PSDs for all three TDI variables, we implemented Welch’s method over 31 segments of the year’s worth of data.

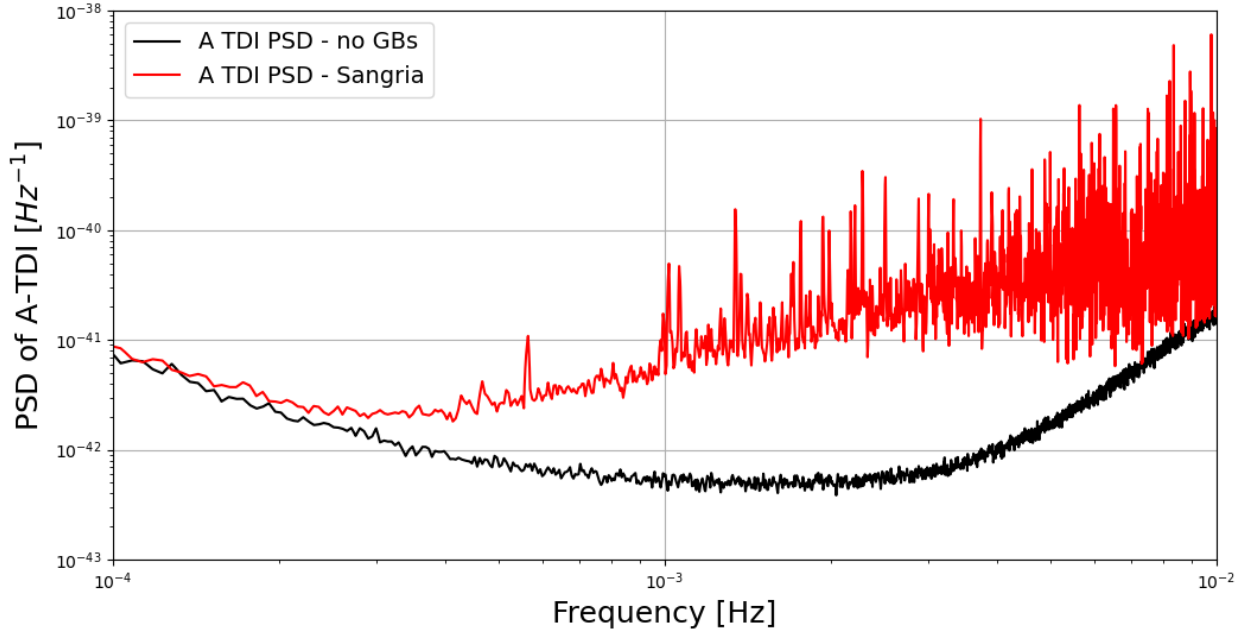


Figure 2. A figure showing the different PSDs we use in the results section. The red curve is the A TDI PSD of the Sangria data and the black curve is the A TDI PSD of Sangria without GBs.

This gave frequency bins with a resolution of 10^{-6} Hz, which were narrow enough to pick up any higher-frequency effects from the GBs. The same number of segments is used to generate all other PSDs for the different analysis stages. Each TDI data stream has a corresponding PSD in all the inference stages.

By constructing the PSDs in this way we have ignored the fact that the PSDs are time-dependent and therefore cannot be stationary. We prioritised the high-frequency information from reading in the entire year’s worth of data with 31 segments instead of a quasi-stationary PSD which is estimated on smaller chunks of data.

4. Results

In this section we present the results of our pipeline. Throughout this section we use one of the six signals found in the Sangria data set, signal 0, as a reference to comment on the overall results of the analysis. The associated data release which contains all of the code and instructions on how to reproduce the results presented can be found in Ref [70]. It also contains the results for the other 5 signals found in Sangria, which we will reference for comparison in this section. Documentation for ongoing developments in PyCBC for LISA related searches and inference can be found in Ref [71].

Signal index	Match
0	0.99749
1	0.99369
2	0.99100
3	0.99612
4	0.99897
5	0.98037

Table 3. The match defined in Equation 2 between the highest SNR template per trigger and the waveforms injected value of the template bank search over the Sangria blind data.

4.1. Search results

To quantify how effective the template bank search was, we computed the match between the highest SNR template per trigger against the injected waveform parameters. All matches are presented in Table 3 for each candidate.

The parameters recovered from the search and the corresponding injected waveform parameters can be found in 4.1. The match for all 6 signals is greater than 0.98. We attempted to produce template banks at higher minimal matches but the time to complete was $\mathcal{O}(\text{days})$ instead of $\mathcal{O}(\text{hours})$ in the 0.7 minimal match case. A template bank search as we have applied it worked exactly how we needed it when considering the balance of computational cost verses accuracy of the returned template.

In the next section, we present our results from the inference. All of the runs in the next section have the reference parameters for the heterodyne likelihood set to the injected parameter values. Running the heterodyne likelihood with the values found in the search gave no significant bias when comparing to inference with the injected parameters are set to the reference values.

Parameters	Injected	Recovered
$m_1 (M_\odot)$	1.76×10^6	1.99×10^6
$m_2 (M_\odot)$	1.30×10^6	1.17×10^6
a_1	0.51	0.74
a_2	0.14	-0.28
$t_c (s)$	6712124	6711638
$\iota (rad)$	1.31	1.35
$\psi (rad)$	1.06	1.22
$\beta (rad)$	-0.35	-0.87
$\lambda (rad)$	2.31	0.37
$\phi_c (rad)$	4.23	4.01

Table 4. Comparison with recovered template parameters verses the injected waveform parameters of signal 0 in the Sangria blind data.

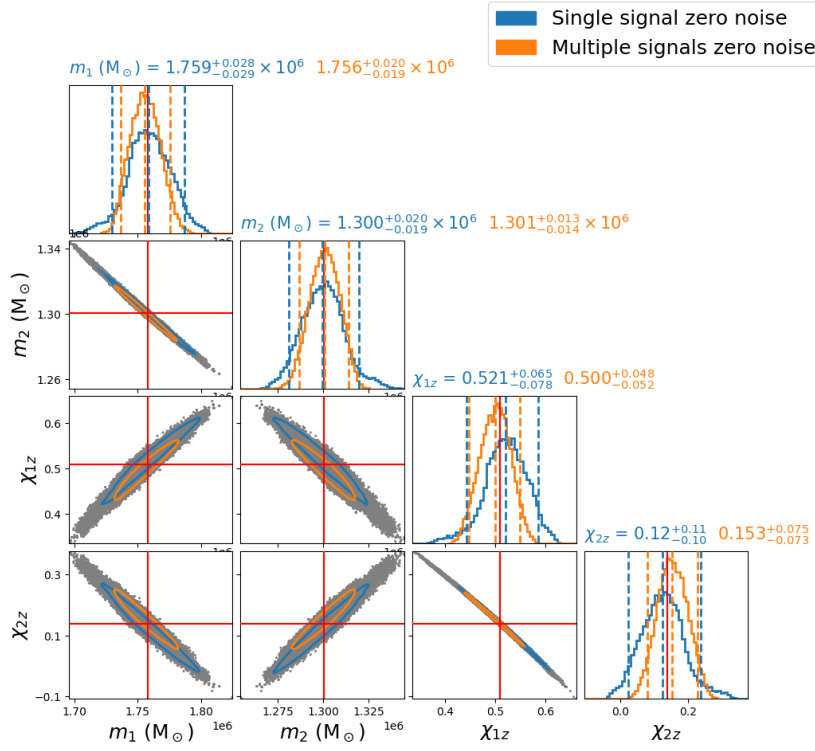


Figure 3. A corner plot showing the recovered intrinsic parameters posteriors of signal 0 in zero noise. The blue curves represent a year's worth of data containing only signal 0. The orange curves represent data containing all 6 signals. The red lines represent the injected parameter values of the signal. The tiles at the top of each column display the median and 90% range for each inference. The contour in the 2D tiles represents the 90% confidence intervals.

4.2. Inference results

When building the inference tools for this challenge, there were several stages of additional complexities which were successively built upon to ensure that each step performed as expected. We performed inference with increasing complexity as follows:

- Injections with BBHx in zero noise.
- Injections with BBHx in Sangria noise without GBs.
- Injections with BBHx in Sangria noise with GBs.
- Sangria blind data.

The difference between the last two bullet points is that the Sangria data has waveform injections that were created with the LDC code base and not injected with BBHx.

We will now present the results of each stage of this development. We will concentrate our discussion on signal 0, the first signal found in Sangria (from time zero); the quoted parameters found in the inference are the maximum log-likelihood sample from the posterior. All of the BBHx inference runs were performed with the heterodyne parameters set to the true injected parameters. The final Sangria runs

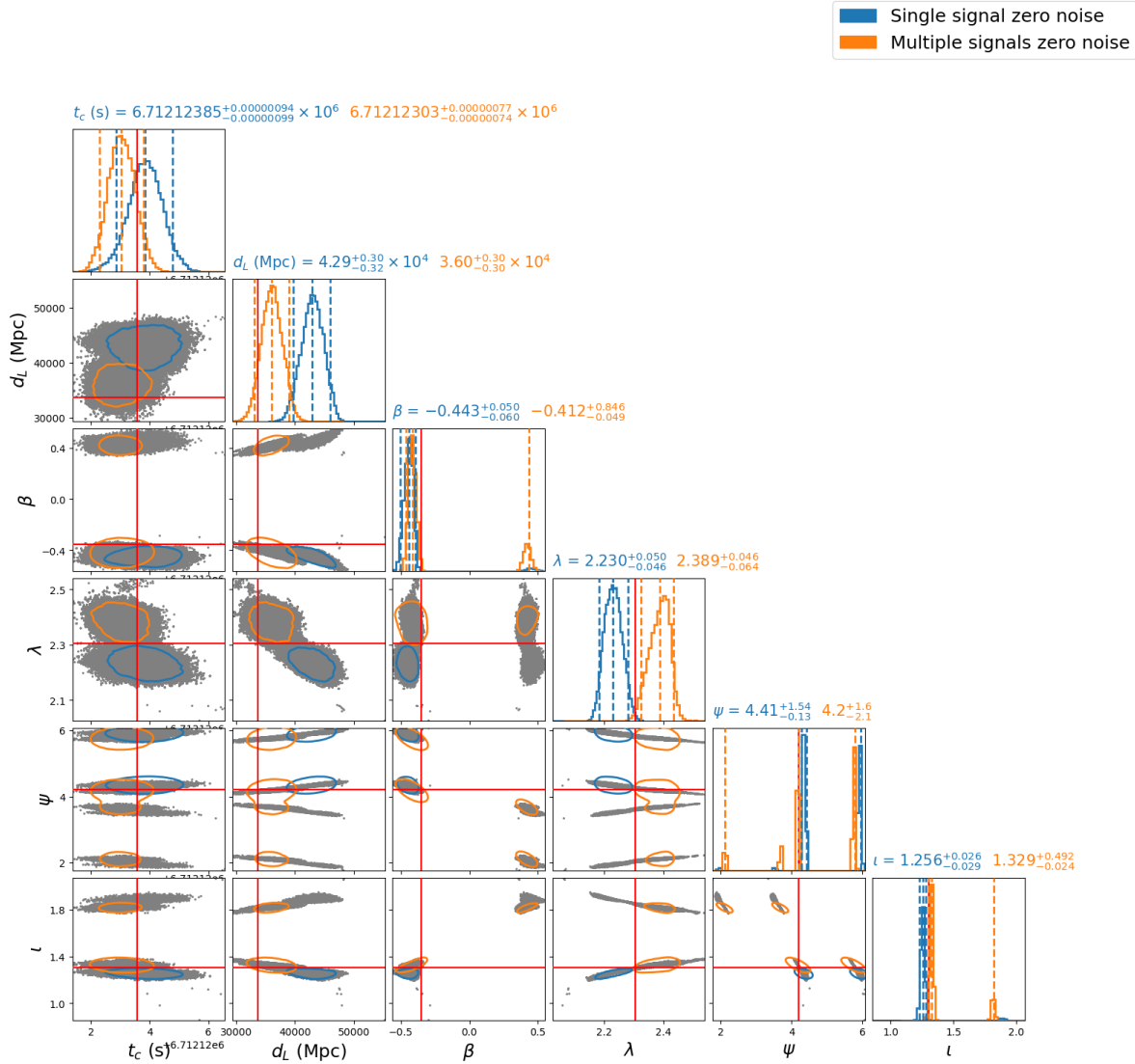


Figure 4. Extrinsic parameter posterior corner plot of injected BBHx signal in zero noise. Red lines represent the injected parameter values of the signal. The tiles at the top of each column display the median and 90% range for each inference. The contour in the 2D tiles represents the 90% confidence intervals.

reference parameters were set to the parameters found in the search section of the pipeline. Figure 2 shows the PSDs used for the first 3 stages before analysing the Sangria blind data. The same sampler settings are used for each analysis to ensure a fair comparison.

For each stage of development, we performed two sets of inference. One set of inference contained only signal 0 injected into the data, shown in blue in subsequent Figures, and the other contained all 6 signals from Sangria, shown in orange. All injections are created in a year's worth of data sampled at 5s intervals to match the convention of the Sangria challenge.

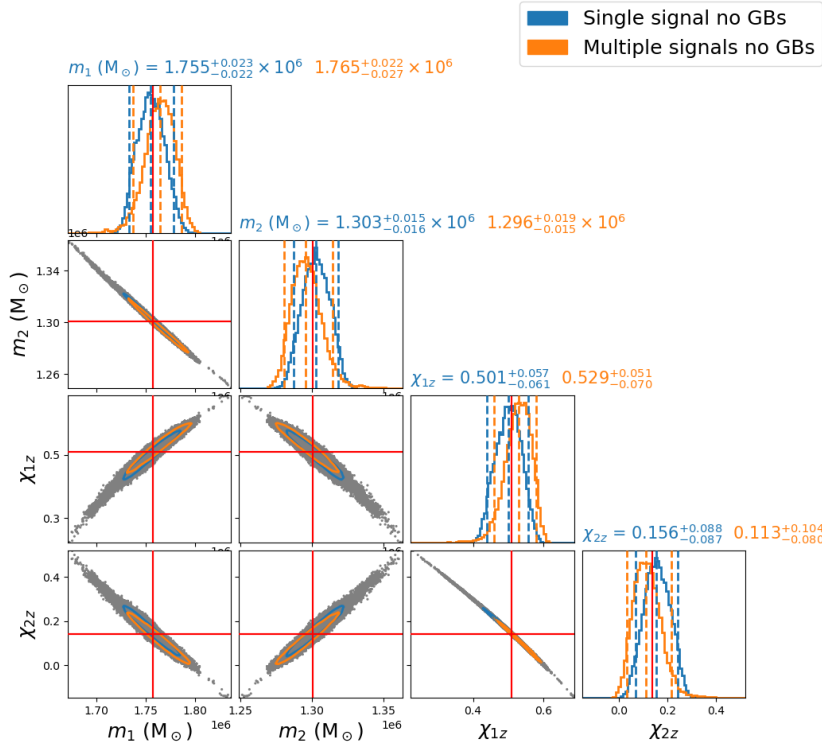


Figure 5. Intrinsic parameter posterior corner plot of injected BBHx signal(s) in Gaussian stationary noise without GBs. Red lines represent the injected parameter values of the signal. The tiles at the top of each column display the median and 90% range for each inference. The contour in the 2D tiles represents the 90% confidence intervals.

4.2.1. Zero noise, BBHx injection - Figure 3 presents the recovered intrinsic parameter posteriors for this analysis, and Figure 4 the extrinsic parameters, along with their 90% confidence intervals. The black PSD curve from Figure 2, was used to scale the signals, to give SNRs of comparable sizes to subsequent analyses. We can see for the single and multiple injection cases that the intrinsic parameters are recovered within the 90% confidence interval of the injected values. However, most extrinsic parameters do not fall within the 90% confidence interval; the sky positions β and λ are recovered well and have found the correct sky mode.

4.2.2. Sangria noise without GBs, BBHx injections - These signals are injected into Gaussian, stationary noise using the Sangria training data. The black curve in Figure 2 is the PSD used for this analysis.

As Figure 5 shows, the inclusion of Gaussian noise when comparing to the zero noise case for both multiple and single injections has no negative bias to the inferred intrinsic parameters. All intrinsic parameters fall within the 90% confidence interval in both cases. The extrinsic parameter recovery, shown in Figure 6, shows no notable differences when comparing to the zero noise case. We do start to see some preference to other likelihood modes in sky position as in two cases (signals 2 and 4) the inference

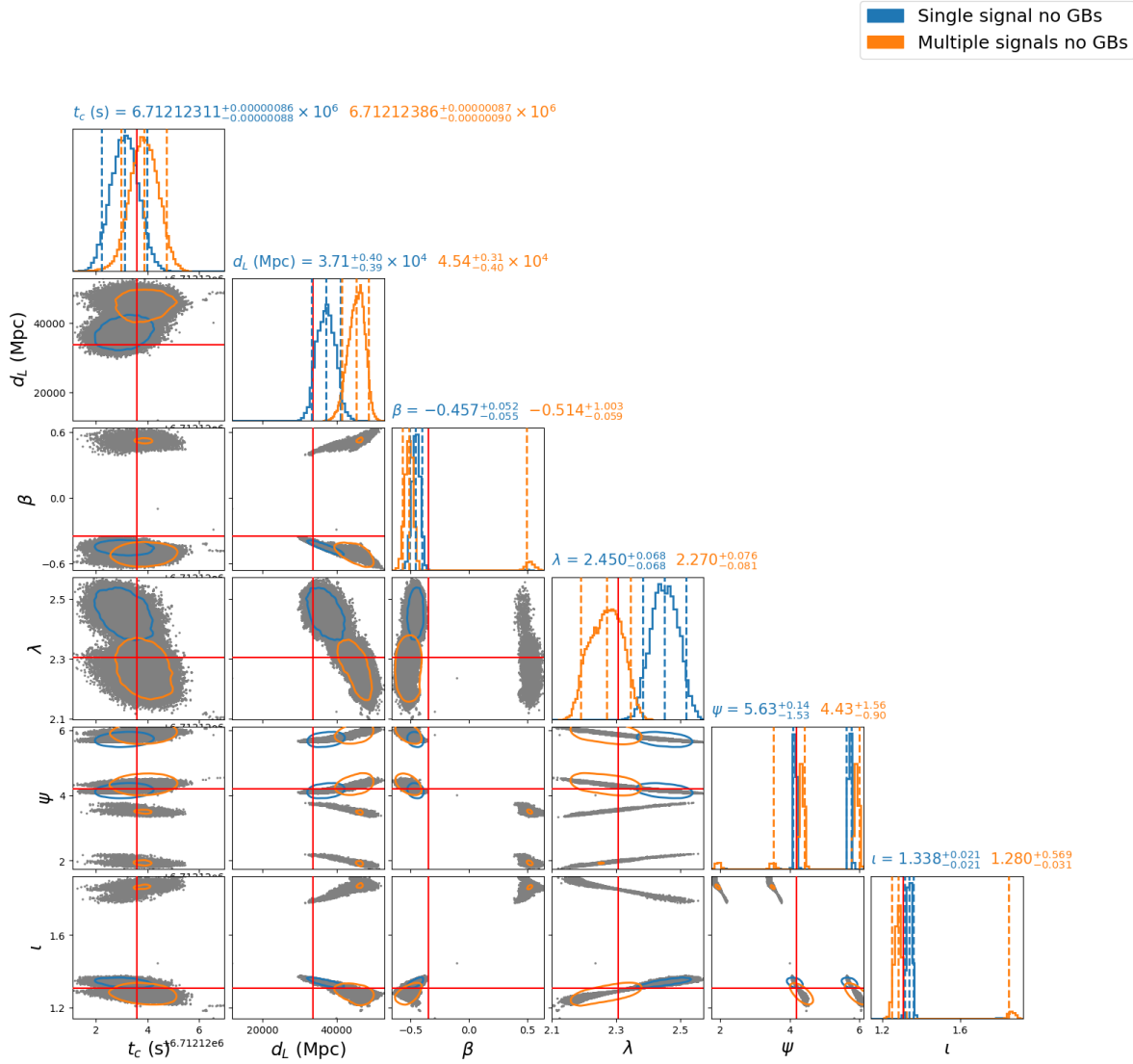


Figure 6. Extrinsic parameter posterior corner plot of injected BBHx signal(s) in Gaussian stationary noise without GBs. Red lines represent the injected parameter values of the signal. The tiles at the top of each column display the median and 90% range for each inference. The contour in the 2D tiles represents the 90% confidence intervals.

preferred the other high likelihood mode of β instead of the true injected mode. This is true in both the single injection case and the multiple injection case.

4.2.3. Sangria noise with GBs, BBHx injections - The red curve in Figure 2 is the PSD used for this section and contains all of the noise from the GBs. We see that this significantly changes the shape of the PSD in the $10^{-3} - 10^{-2} Hz$ region of frequency space.

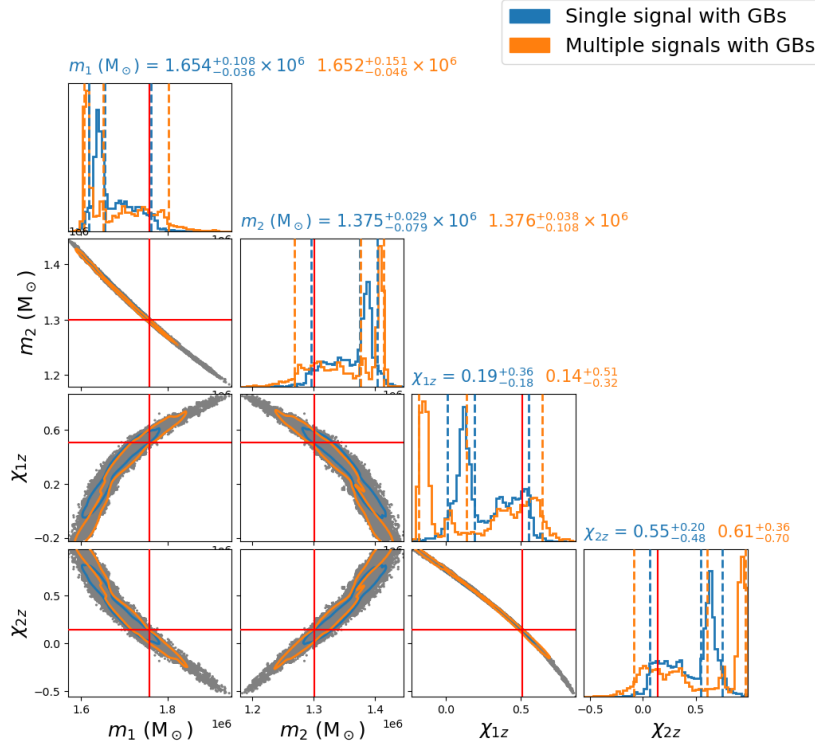


Figure 7. Intrinsic parameter posterior corner plot of injected BBHx signal(s) in Gaussian stationary noise with GBs. Red lines represent the injected parameter values of the signal. The tiles at the top of each column display the median and 90% range for each inference. The contour in the 2D tiles represents the 90% confidence intervals.

The posteriors in Figures 7 and 8 are broader which is expected given the noise curve with GBs present. Figure 7 demonstrates that the intrinsic parameters still fall within the 90% confidence interval.

GBs have had the most significant effect on inference thus far as the peaks in the posterior likelihood have shifted from the injected value when compared to the no GBs case. We also see a lot more structure in the posteriors that includes GBs. In Table 4 we have calculated the percentage of samples from the posterior with a higher

Signal	Sangria noise without GBs	Sangria noise with GBs	Sangria blind
0	78%	34%	93%
1	41%	84%	98%
2	20%	44%	99%
3	2.7%	84%	100%
4	36%	84%	81%
5	18%	6.7%	86%

Table 5. Each percentage represents the amount of samples whose likelihood value is greater than the likelihood of the corresponding injected waveform.

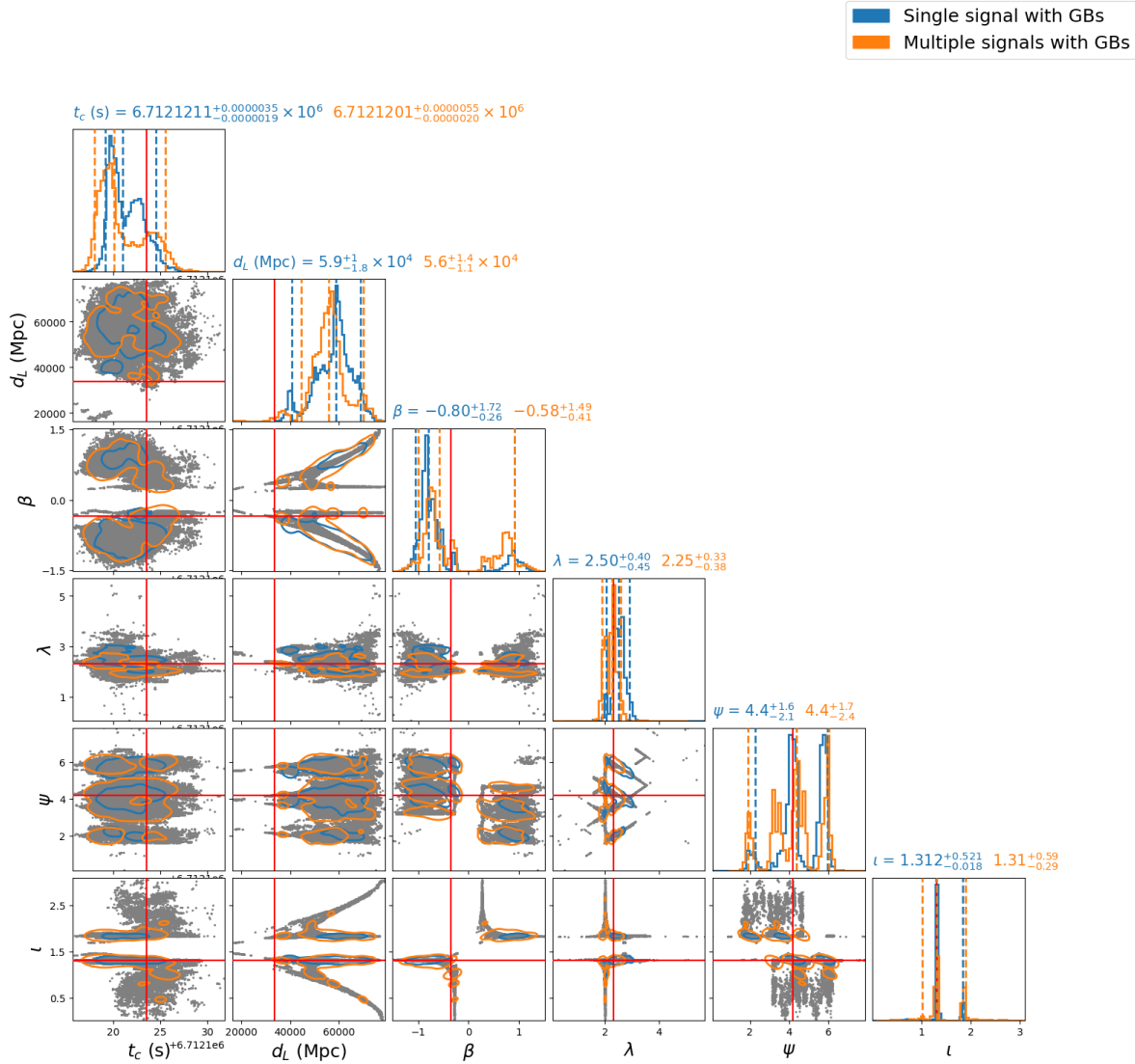


Figure 8. Extrinsic parameter posterior corner plot of injected BBHx signal(s) in Gaussian stationary noise with GBs. Red lines represent the injected parameter values of the signal. The tiles at the top of each column display the median and 90% range for each inference. The contour in the 2D tiles represents the 90% confidence intervals.

likelihood than that of the likelihood of the injected waveform. If the assumptions of Gaussianity and stationarity are valid, these values for a collection of posteriors from different signals/injections should be uniformly distributed. We see for the case of Gaussian stationary noise without GBs that the distribution of values does appear to be uniform, whereas this is no longer the case when including GBs. The effect of GBs being non-stationary therefore has biased the inferred parameters away from the injected value. The test performed here would have benefited from $\mathcal{O}(100)$ posteriors to properly conclude that the distribution is uniform. Even with only six signals we can clearly see the bias when the data contains GBs and when inspecting the full Sangria data.

Signal 0		
Parameters	Injected value	Recovered value
$m_1 (M_\odot)$	1.76×10^6	$1.70^{+0.13}_{-0.11} \times 10^6$
$m_2 (M_\odot)$	1.30×10^6	$1.34^{+0.83}_{-0.89} \times 10^6$
a_1	0.51	$0.39^{+0.32}_{-0.56}$
a_2	0.14	$0.29^{+0.66}_{-0.49}$
$t_c (s)$	6712124	6712466^{+103}_{-793}
$\iota (rad)$	1.31	$1.32^{+0.52}_{-0.02}$
$\psi (rad)$	1.06	$1.44^{+1.03}_{-1.08}$
$\beta (rad)$	-0.35	$-0.05^{+0.77}_{-0.59}$
$\lambda (rad)$	2.31	$2.11^{+2.40}_{-0.79}$

Table 6. The injected and recovered parameters for signal 0 in the blind Sangria dataset. The recovered values are stated with the 90% confidence regions.

As for the extrinsic parameters for signal 0, the inferred values represent the injected waveform well. This is not true for the other signals in the data as most struggle to find the correct sky mode for β and/or λ .

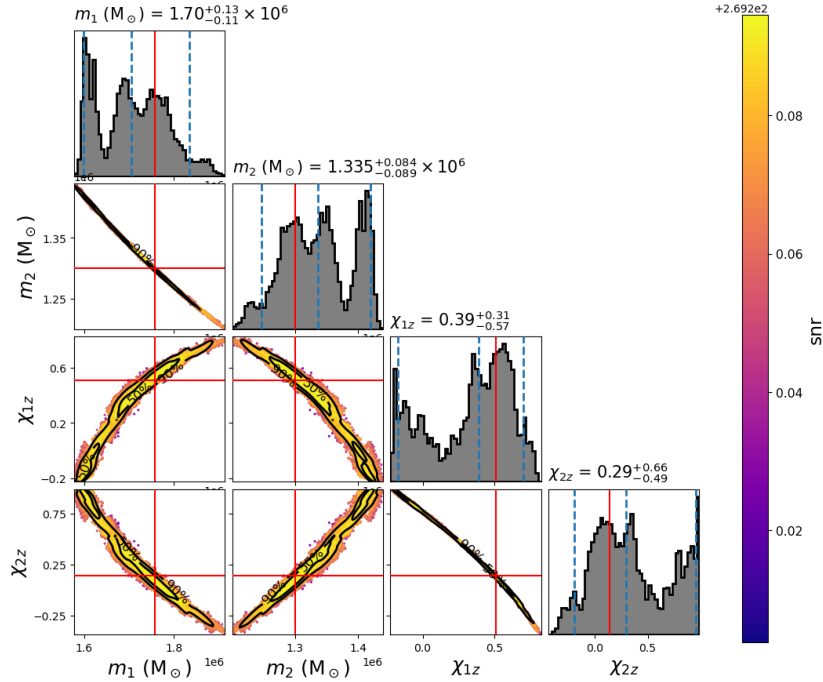


Figure 9. Intrinsic parameter posterior corner plot of Sangria blind data for signal 0. Red lines represent the injected parameter values of the signal. The tiles at the top of each column display the median and 90% range for each inference. The contour in the 2D tiles represents the 90% confidence intervals.

4.2.4. *Sangria blind* - The full parameter recovery of signal 0 in Sangria is presented, along with the signals injected parameters in Table 5. The intrinsic parameters shown in Figure 9, fall within the 90% confidence interval, however this is not true for all signals in the data set. There is one case where all intrinsic parameters peak at roughly the 88% confidence interval. Overall, the peaks in likelihood are far less prominent when compared to the previous cases.

Extrinsic parameters also have far less prominent peaks than previous cases and suffer from the same sky resolution issues where the wrong mode is commonly favoured. For half of the cases, D_L is recovered within the 90% interval and for all cases, t_c and ι are recovered in the 90% confidence interval.

Figure 10 shows the extrinsic recovery of our reference signal and is the only example out of the six signals that recovers the correct mode for λ . There is no special reason

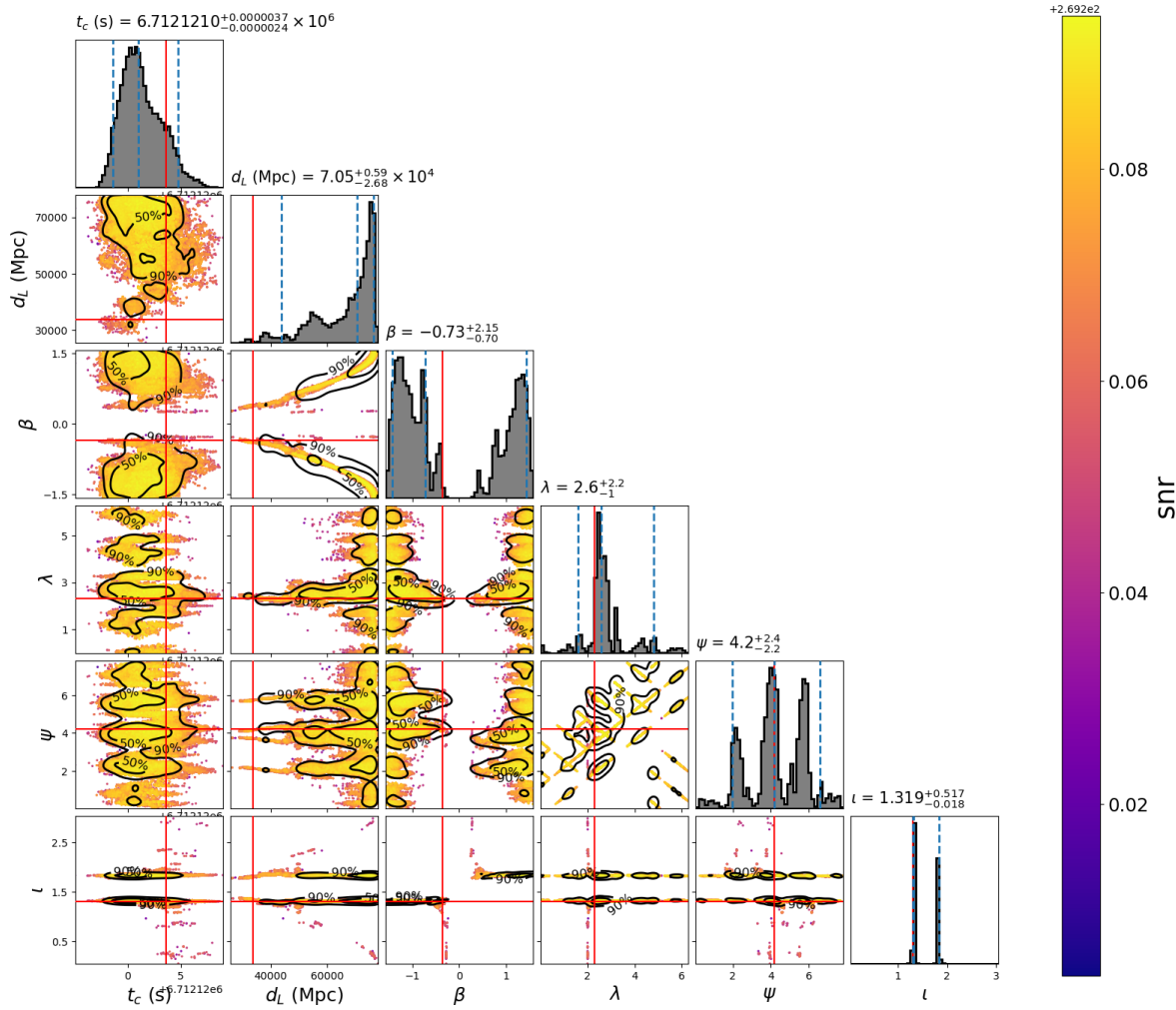


Figure 10. Extrinsic parameter posterior corner plot of Sangria blind data for signal 0. Red lines represent the injected parameter values of the signal. The tiles at the top of each column display the median and 90% range for each inference. The contour in the 2D tiles represents the 90% confidence intervals.

for this, but it reinforces how difficult it is to find the correct likelihood peak in sky position.

5. Conclusion

The application of a template bank search was able to identify all MBHB signals in the Sangria mock data challenge. Although the search for MBHB signals is relatively trivial due to the high SNR, being able to provide reference parameters for the heterodyne likelihood is the main advantage when taking this approach. The template bank took $\mathcal{O}(\text{hours})$ to produce with a relatively low number of templates to fulfill a minimal match of 0.7. Given that the SNR recovered is greater than 98%, we find that this technique is a viable approach to quickly search through LISA data for MBHBs and at the same time provide appropriately high likelihood reference parameters for heterodyning to not bias parameter estimation.

We have shown that the introduction of different forms of noise can have an effect on both intrinsic and extrinsic parameter recovery, although the extrinsic parameter recovery suffers more than the intrinsic. Something to consider about this data set is how the injected signals only contain the dominant (2,2) mode. Other works have shown that sky position recovery is vastly improved as other sub dominant modes are introduced to parameter estimation [59]. A further study could be to investigate the inference of a multi-modal signal, in the presence of LISA instrumental noise. We could then go further by introducing non-stationarities in the data, with the inclusion of GBs.

The intrinsic parameter recovery of MBHBs in the presence of confusion noise caused by GBs can bias the result away from the true value. Although the injected values in our work did fall within the 90% confidence intervals, the peak likelihood has moved away from the injected value when compared to the no GB inference case, see Figures 5 and 7. This motivates the need for a full global fit pipeline, that can identify and infer the properties of the GBs and then remove them from the data before running inference on MBHBs. This was first described in Ref [13].

An area of further investigation concerns how we estimate PSDs. As stated previously, in this work we estimate our PSDs by reading in the entire year's worth of data. Due to LISA's motion across the sky, this makes the PSDs non-stationary. One possible method is to construct our PSD by assuming quasi-stationarity on smaller time chunks of the year's worth of data, and assemble these into one PSD using the time/frequency track of the reference signal in question. It would also be interesting to investigate what effects the PSD being non-stationary has on the search and inference of such high SNR signals.

6. Acknowledgements

We would like to thank Stas Babak, Quentin Baghi, Maude Le Jeune, Jean-Baptiste Bayle, and Natalia Korsakova for helpful discussions regarding LISA data analysis. We

also thank Michael Katz for help with using BBHx and for making his code publicly available for use. We also thank the GW group at the University of Portsmouth for their discussion and support during the project. CW would like to particularly thank Gareth Cabourn Davies and Arthur Tolley for their constant advice and feedback. We are grateful to the computing teams from the University of Portsmouth and AEI Hannover for their significant technical support. CW is supported by a STFC studentship. LKN acknowledges support from the UKRI Future Leaders Fellowship through grant MR/T01881X/1. IWH and LKN acknowledge support from the UK Space Agency through grant ST/X002225/1. Numerical computations were done on the Sciama High Performance Compute (HPC) cluster which is supported by the ICG, SEPNet and the University of Portsmouth.

References

- [1] Amaro-Seoane P *et al* (LISA) 2017 (*Preprint* 1702.00786)
- [2] Wise J H 2023 (*Preprint* 2304.09311)
- [3] Stokov V, Fragione G and Berti E 2023 (*Preprint* 2303.00015)
- [4] Barack L and Pound A 2019 *Rept. Prog. Phys.* **82** 016904 (*Preprint* 1805.10385)
- [5] Gair J R, Babak S, Sesana A, Amaro-Seoane P, Barausse E, Berry C P L, Berti E and Sopuerta C 2017 *J. Phys. Conf. Ser.* **840** 012021 (*Preprint* 1704.00009)
- [6] Barausse E *et al.* 2020 *Gen. Rel. Grav.* **52** 81 (*Preprint* 2001.09793)
- [7] Li K, Bogdanović T, Ballantyne D R and Bonetti M 2022 *Astrophys. J.* **933** 104 (*Preprint* 2201.11088)
- [8] Li K, Bogdanović T, Ballantyne D R and Bonetti M 2022 (*Preprint* 2207.14231)
- [9] Steinle N, Middleton H, Moore C J, Chen S, Klein A, Pratten G, Buscicchio R, Finch E and Vecchio A 2023 (*Preprint* 2305.05955)
- [10] Fang Y and Yang H 2022 (*Preprint* 2209.14509)
- [11] 2023 (the new) LISA data challenge - Available online at: <https://lisa-ldc.lal.in2p3.fr/>, last accessed on 13.06.2023
- [12] Baghi Q (LDC Working Group) 2022 The LISA Data Challenges *56th Rencontres de Moriond on Gravitation* (*Preprint* 2204.12142)
- [13] Cornish N J and Crowder J 2005 *Phys. Rev. D* **72** 043005 (*Preprint* gr-qc/0506059)
- [14] Vallisneri M 2009 *Class. Quant. Grav.* **26** 094024 (*Preprint* 0812.0751)
- [15] Karnesis N, Katz M L, Korsakova N, Gair J R and Stergioulas N 2023 (*Preprint* 2303.02164)
- [16] Bayle J B, Hartwig O, Lilley M, Hees A, Chapman-Bird C, Woan G and Wolf P 2023 End-to-end simulation and analysis pipeline for LISA *57th Rencontres de Moriond on Gravitation* (*Preprint* 2305.09702)
- [17] Cornish N J and Hellings R W 2003 *Class. Quant. Grav.* **20** 4851–4860 (*Preprint* gr-qc/0306096)
- [18] Rubbo L J, Cornish N J and Poujade O 2004 *Phys. Rev. D* **69** 082003 (*Preprint* gr-qc/0311069)
- [19] Petiteau A, Auger G, Halloin H, Jeannin O, Plagnol E, Pireaux S, Regimbau T and Vinet J Y 2008 *Phys. Rev. D* **77** 023002 (*Preprint* 0802.2023)
- [20] Littenberg T B and Cornish N J 2023 *Phys. Rev. D* **107** 063004 (*Preprint* 2301.03673)
- [21] Bayle J B and Hartwig O 2023 *Phys. Rev. D* **107** 083019 (*Preprint* 2212.05351)
- [22] Digman M C and Cornish N J 2022 *Astrophys. J.* **940** 10 (*Preprint* 2206.14813)
- [23] 2023 LISA data challenge 2a: Sangria - Available online at: <https://lisa-ldc.lal.in2p3.fr/challenge2a>, last accessed on 13.06.2023
- [24] 2023 LISA data challenge 2a, Sangria manual - Available online at: <https://lisa-ldc.lal.in2p3.fr/static/data/pdf/LDC-manual-Sangria.pdf>, last accessed on 13.06.2023

- [25] Nelemans G, Yungelson L R and Portegies Zwart S F 2001 *Astron. Astrophys.* **375** 890–898 (*Preprint astro-ph/0105221*)
- [26] Finch E, Bartolucci G, Chucherko D, Patterson B G, Korol V, Klein A, Bandopadhyay D, Middleton H, Moore C J and Vecchio A 2023 *Mon. Not. Roy. Astron. Soc.* **522** 5358–5373 (*Preprint 2210.10812*)
- [27] Husa S, Khan S, Hannam M, Pürrer M, Ohme F, Jiménez Forteza X and Bohé A 2016 *Phys. Rev. D* **93** 044006 (*Preprint 1508.07250*)
- [28] Khan S, Husa S, Hannam M, Ohme F, Pürrer M, Jiménez Forteza X and Bohé A 2016 *Phys. Rev. D* **93** 044007 (*Preprint 1508.07253*)
- [29] Maggiore M 2008 *Gravitational waves: Volume 1: Theory and experiments* vol 1 (Oxford university press)
- [30] Shaddock D A, Tinto M, Estabrook F B and Armstrong J W 2003 *Phys. Rev. D* **68** 061303 (*Preprint gr-qc/0307080*)
- [31] Tinto M, Estabrook F B and Armstrong J W 2004 *Phys. Rev. D* **69** 082001 (*Preprint gr-qc/0310017*)
- [32] Arnaud K A *et al.* 2006 *AIP Conf. Proc.* **873** 619–624 (*Preprint gr-qc/0609105*)
- [33] Babak S *et al.* (Mock LISA Data Challenge Task Force) 2010 *Class. Quant. Grav.* **27** 084009 (*Preprint 0912.0548*)
- [34] Arnaud K A *et al.* 2007 *Class. Quant. Grav.* **24** S551–S564 (*Preprint gr-qc/0701170*)
- [35] PyCBC Development Team and the LIGO / Virgo Collaborations 2023 PyCBC - Available online at: <https://pycbc.org/>, last accessed on 13.06.2023
- [36] Abbott B P *et al.* (LIGO, VIRGO) 2017 *Observation of Gravitational Waves from a Binary Black Hole Merger* pp 291–311
- [37] Usman S A *et al.* 2016 *Class. Quant. Grav.* **33** 215004 (*Preprint 1508.02357*)
- [38] Biwer C M, Capano C D, De S, Cabero M, Brown D A, Nitz A H and Raymond V 2019 *Publ. Astron. Soc. Pac.* **131** 024503 (*Preprint 1807.10312*)
- [39] Nitz A, Harry I, Brown D, Biwer C M, Willis J, Canton T D, Capano C, Dent T, Pekowsky L, Williamson A R, De S, Cabero M, Machenschalk B, Macleod D, Kumar P, Reyes S, dfinstad, Pannarale F, Kumar S, Massinger T, Tápai M, Singer L, Davies G S C, Khan S, Fairhurst S, Nielsen A, Singh S, Chandra K, shasvath and veronica villa 2022 gwastro/pycbc: v2.0.2 release of pycbc URL <https://doi.org/10.5281/zenodo.6324278>
- [40] Allen B 2005 *Phys. Rev. D* **71** 062001 (*Preprint gr-qc/0405045*)
- [41] Abbott R *et al.* (LIGO Scientific, VIRGO) 2021 (*Preprint 2108.01045*)
- [42] Abbott R *et al.* (LIGO Scientific, VIRGO, KAGRA) 2021 (*Preprint 2111.03606*)
- [43] Nitz A H, Kumar S, Wang Y F, Kastha S, Wu S, Schäfer M, Dhurkunde R and Capano C D 2023 *Astrophys. J.* **946** 59 (*Preprint 2112.06878*)
- [44] Helstrom C W 1968 *Statistical theory of signal detection* (Pergamon Press)
- [45] Dent T and Veitch J 2014 *Phys. Rev. D* **89** 062002 (*Preprint 1311.7174*)
- [46] Owen B J 1996 *Phys. Rev. D* **53** 6749–6761 (*Preprint gr-qc/9511032*)
- [47] Owen B J and Sathyaprakash B S 1999 *Phys. Rev. D* **60** 022002 (*Preprint gr-qc/9808076*)
- [48] Babak S, Balasubramanian R, Churches D, Cokelaer T and Sathyaprakash B S 2006 *Class. Quant. Grav.* **23** 5477–5504 (*Preprint gr-qc/0604037*)
- [49] Keppel D 2013 *Phys. Rev. D* **87** 124003 (*Preprint 1303.2005*)
- [50] Privitera S, Mohapatra S R P, Ajith P, Cannon K, Fotopoulos N, Frei M A, Hanna C, Weinstein A J and Whelan J T 2014 *Phys. Rev. D* **89** 024003 (*Preprint 1310.5633*)
- [51] Davies G S, Dent T, Tápai M, Harry I, McIsaac C and Nitz A H 2020 *Phys. Rev. D* **102** 022004 (*Preprint 2002.08291*)
- [52] Cornish N J 2010 (*Preprint 1007.4820*)
- [53] Zackay B, Dai L and Venumadhav T 2018 (*Preprint 1806.08792*)
- [54] Biwer C M, Capano C D, De S, Cabero M, Brown D A, Nitz A H and Raymond V 2019 *Publ. Astron. Soc. Pac.* **131** 024503 (*Preprint 1807.10312*)

- [55] Katz M L, Marsat S, Chua A J K, Babak S and Larson S L 2020 *Phys. Rev. D* **102** 023033 (*Preprint* 2005.01827)
- [56] Katz M L 2022 *Phys. Rev. D* **105** 044055 (*Preprint* 2111.01064)
- [57] Katz M 2021 mikekatz04/bbhx: First official public release 10.5281/zenodo.5730688
- [58] Marsat S and Baker J G 2018 (*Preprint* 1806.10734)
- [59] Marsat S, Baker J G and Dal Canton T 2021 *Phys. Rev. D* **103** 083011 (*Preprint* 2003.00357)
- [60] London L *et al* 2018 *Phys. Rev. Lett.* **120** 161102 (*Preprint* 1708.00404)
- [61] Husa S, Khan S, Hannam M, Pürrer M, Ohme F, Jiménez Forteza X and Bohé A 2016 *Phys. Rev. D* **93** 044006 (*Preprint* 1508.07250)
- [62] Khan S, Husa S, Hannam M, Ohme F, Pürrer M, Jiménez Forteza X and Bohé A 2016 *Phys. Rev. D* **93** 044007 (*Preprint* 1508.07253)
- [63] London L *et al* 2018 *Phys. Rev. Lett.* **120** 161102 (*Preprint* 1708.00404)
- [64] Tinto M and Dhurandhar S V 2005 *Living Rev. Rel.* **8** 4 (*Preprint* gr-qc/0409034)
- [65] Babak S 2008 *Class. Quant. Grav.* **25** 195011 (*Preprint* 0801.4070)
- [66] Harry I W, Allen B and Sathyaprakash B S 2009 *Phys. Rev. D* **80** 104014 (*Preprint* 0908.2090)
- [67] Ajith P, Fotopoulos N, Privitera S, Neunzert A and Weinstein A J 2014 *Phys. Rev. D* **89** 084041 (*Preprint* 1210.6666)
- [68] Speagle J S 2020 *Mon. Not. Roy. Astron. Soc.* **493** 3132–3158 (*Preprint* 1904.02180)
- [69] Blanchet L, Damour T, Iyer B R, Will C M and Wiseman A G 1995 *Phys. Rev. Lett.* **74** 3515–3518 (*Preprint* gr-qc/9501027)
- [70] Weaving, C R and Wu, S. GitHub to mbhbs-with-pycbc. <https://github.com/gwastro/mbhbs-with-pycbc>
- [71] 2023 LISA parameter estimation for simulated massive black hole binary - Available online at: http://pycbc.org/pycbc/latest/html/inference/examples/lisa_smbhb_ldc_pe.html, last accessed on 13.06.2023